Accepted Manuscript

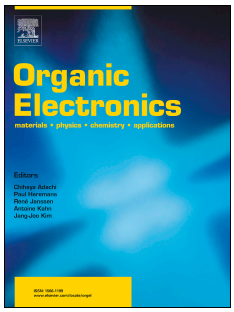

Investigating the molecular orientation of $Ir(ppy)_3$ and $Ir(ppy)_2(acac)$ emitter complexes by X-ray diffraction

Caroline Murawski, Chris Elschner, Simone Lenk, Sebastian Reineke, Malte C. Gather

PII: S1566-1199(17)30568-2

DOI: 10.1016/j.orgel.2017.11.036

Reference: ORGELE 4411

To appear in: *Organic Electronics*

Received Date: 25 July 2017

Revised Date: 6 October 2017

Accepted Date: 24 November 2017

Please cite this article as: C. Murawski, C. Elschner, S. Lenk, S. Reineke, M.C. Gather, Investigating the molecular orientation of $Ir(ppy)_3$ and $Ir(ppy)_2(acac)$ emitter complexes by X-ray diffraction, *Organic Electronics* (2017), doi: 10.1016/j.orgel.2017.11.036.

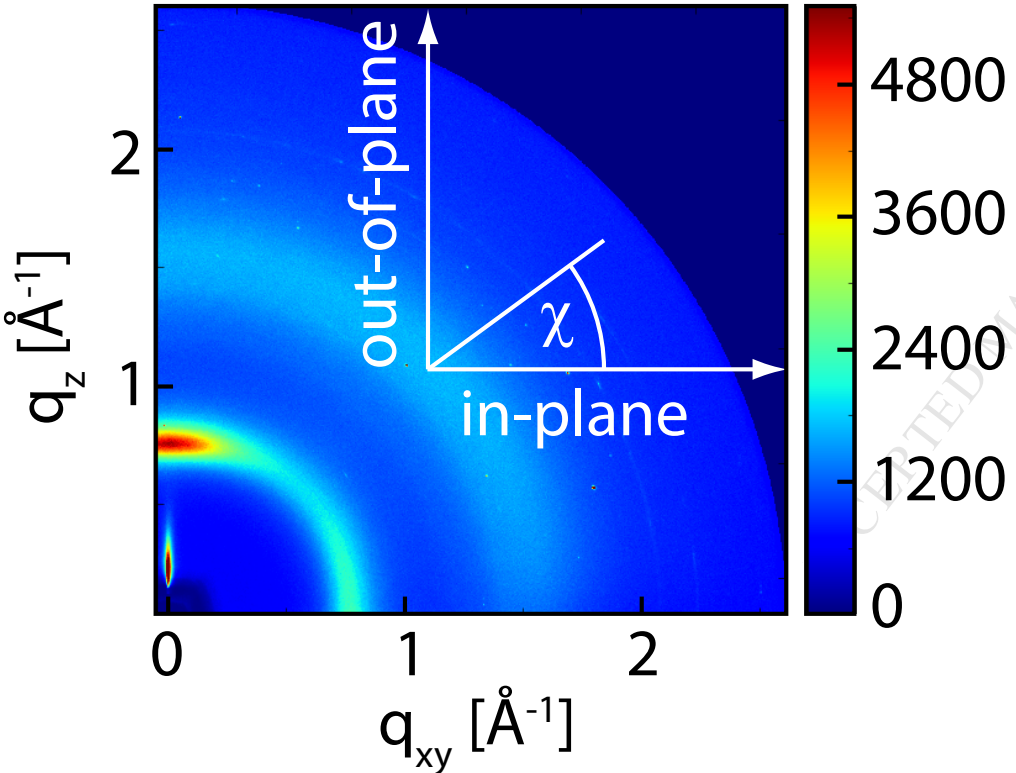

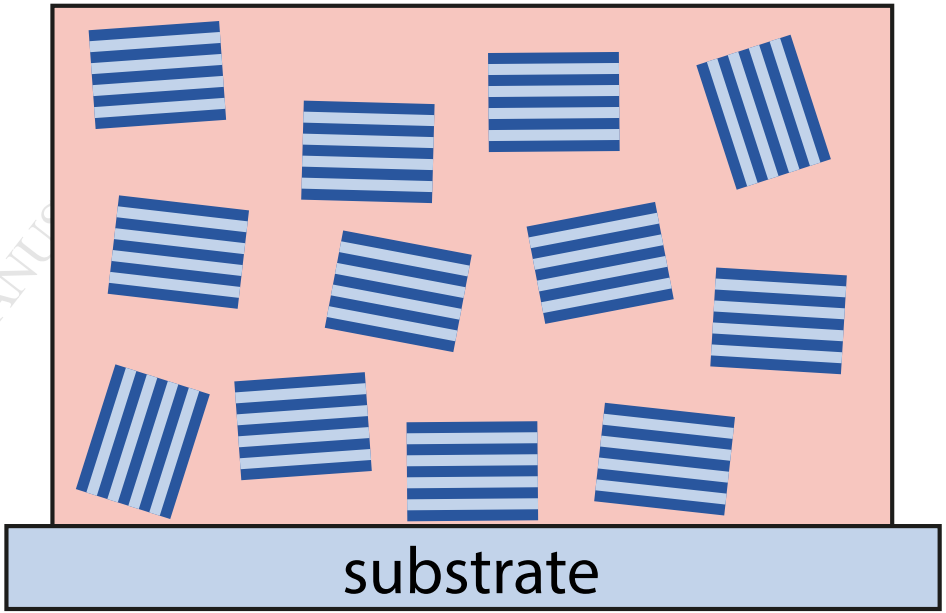

Investigating the molecular orientation of $Ir(ppy)_3$ and $Ir(ppy)_2(acac)$ emitter complexes by X-ray diffraction

Caroline Murawski[1,2], Chris Elschner[1], Simone Lenk[1], Sebastian Reineke[1], and Malte C. Gather[1,2,]*

[1] Dresden Integrated Center for Applied Physics and Photonic Materials (IAPP) and Institute for Applied Physics, Technische Universität Dresden, Nöthnitzer Str. 61, 01187 Dresden, Germany

[2] Organic Semiconductor Centre, SUPA, School of Physics & Astronomy, University of St Andrews, North Haugh, St Andrews, KY16 9SS, Scotland, UK

*mcg6@st-andrews.ac.uk (Corresponding Author)

ABSTRACT. We study thermally evaporated thin films of $Ir(ppy)_3$ and $Ir(ppy)_2(acac)$ by means of grazing incidence X-ray diffraction (GIXRD) and grazing incidence wide-angle X-ray scattering (GIWAXS). $Ir(ppy)_3$ and $Ir(ppy)_2(acac)$ are both widely used as phosphorescent green emitter molecules in organic light-emitting diodes (OLEDs) and it was previously found that differences in their average transition dipole orientation affect the light extraction efficiency in OLEDs. Here we show that in pure films both materials form crystalline grains and that these grains exhibit a preferred orientation with respect to the substrate. When doped into an

amorphous host, both the orientation and formation of the crystallites remain nearly unchanged for the concentration range accessible with GIXRD and GIWAXS. This is remarkable given that the transition dipole moments have found to be oriented only for $Ir(ppy)_2(acac)$ but isotropic for $Ir(ppy)_3$. Analysis of the crystallite size indicates that the tendency to form crystallites is stronger for $Ir(ppy)_3$ than for $Ir(ppy)_2(acac)$. From a comparison of the thin-film diffraction data of $Ir(ppy)_3$ to its powder pattern, we infer that $Ir(ppy)_3$ molecules are oriented with their permanent dipole moment roughly parallel to the substrate. Our findings will guide the further understanding of the mechanisms controlling transition dipole orientation and may thus lead to further improvements in device efficiency.

KEYWORDS. Phosphorescent iridium complex, orientation, organic light-emitting diode, X-ray diffraction.

1. Introduction

The orientation of the emitting molecules in organic light-emitting diodes (OLEDs) has a significant impact on OLED efficiency.[1–5] In particular, if all transition dipole moments are aligned horizontally with respect to the substrate, one expects an increase in outcoupling efficiency by approximately 60% compared to isotropic orientation.[6] A preferential orientation of the transition dipole moment has been observed for many emitting molecules but its origin remains a subject of debate in the OLED community. Graf *et al.* suggested that strong dipole-dipole potential of iridium compounds leads to aggregation and, thus, random orientation, while the observed anisotropy of emitters with a weaker potential is based on matrix-induced London forces.[7] A study by Kim *et al.* found that the symmetry axes of all investigated emitters were

preferentially aligned with respect to the substrate due to the formation of supramolecules with the host materials.[6] Recently, Jurow *et al.* suggested that the strong chemical asymmetry that is often observed in heteroleptic emitter complexes means that molecules adopt a preferential orientation with respect to the substrate when they impinge on the film surface during thermal evaporation.[8]

So far, there is a lack of experimental data on the alignment of the molecules themselves (i.e. the average orientation of the principal axes of symmetry) because the quantity that has been measured in most experiments so far is the average orientation of the transition dipole moments in the film with respect to the substrate. Typical measurement techniques include variable angle spectroscopic ellipsometry[4] and angular resolved photoluminescence[9,10] and electroluminescence[3,7] measurements. While molecules that show a predominant orientation of their transition dipoles will automatically have a preferred orientation of their symmetry axis, the situation is less clear for molecules that show an isotropic dipole orientation when characterized with the above optical methods. For these molecules, the observed isotropy can either be due to random orientation of the molecule or may be indicative of a situation where molecules are aligned on the substrate but have their transition dipole moments slanted such that they contribute equally in all three emission directions.[6,11]

Very recently, X-ray diffraction studies have shown that phosphorescent platinum emitters can form large crystals with a nearly perfect horizontal alignment of the transition dipoles.[12] In contrast, the light-emitting structures that are traditionally used in OLEDs are generally believed to comprise of amorphous films which are generally not amenable to investigation by X-ray diffraction. Therefore, structure analysis by means of X-ray diffraction has mainly been applied to organic semiconductors in order to evaluate charge and exciton transport in thin-film

transistors or photovoltaics where crystalline or semi-crystalline morphology is more prevalent.[13–15] In this contribution, we use X-ray diffraction measurements to determine the orientation of the symmetry axes of $Ir(ppy)_3$ and $Ir(ppy)_2(acac)$ molecules and, thus, their alignment on a substrate. $Ir(ppy)_3$ and $Ir(ppy)_2(acac)$ are selected as model emitters because they are well-studied in terms of their transition dipole orientation and their tendency to form aggregates.[3,16] We have previously found that in a CBP matrix the transition dipoles of $Ir(ppy)_2(acac)$ exhibit a preferential horizontal orientation with an anisotropy factor of $a = 0.23$ while the transition dipoles of $Ir(ppy)_3$ showed isotropic orientation ($a = 0.33$).[3] (The anisotropy factor a is defined as the ratio of vertical transition dipole moments to the total radiated power, i.e. $a = 0$ represents perfect horizontal orientation.)

When X-ray diffraction measurements are performed in conventional specular geometry, i.e. the incident angle ω equals the reflection angle 2θ, the penetration depth of X-rays into the surface of the sample is several µm, which is orders of magnitude larger than the typical layer thickness of organic thin films. In order to get information about the organic films and to not predominantly probe the underlying substrate, grazing-incidence geometries are used here, i.e. the angle ω between the incident X-rays and sample surface is kept very small ($\omega \approx 0.2°$). This leads to total reflection at the interface between the organic thin film and substrate and thus allows probing solely the organic material.

2. Experimental Section

Layer fabrication. Tris(2-phenylpyridine)iridium(III) ($Ir(ppy)_3$) and bis(2-phenylpyridine)(acetylacetonate)iridium(III) ($Ir(ppy)_2(acac)$) were deposited either as neat films

or doped into 4,4',4"-tris(N-carbazolyl)-triphenylamine (TCTA) or 4,4'-bis(carbazol-9-yl)biphenyl (CBP) using co-evaporation. All materials were purchased commercially and purified further by vacuum sublimation prior to use. 50 nm thick organic films were prepared on pre-cleaned glass substrates by thermal evaporation in UHV at a base pressure of 10^{-7} mbar (Kurt J. Lesker Co.). The host materials were deposited at rates between 0.3 and 0.8 Å/s. For co-evaporation, the deposition rate of the dopant was adjusted to achieve the desired doping concentration. The rates and layer thicknesses were controlled in-situ by calibrated quartz crystal monitors. Samples were packed into sealed boxes under nitrogen atmosphere directly after fabrication and boxes were only opened immediately before the measurement to avoid extended exposure of the films to air.

X-ray diffraction measurements. Two different configurations were employed – grazing incidence X-ray diffraction (GIXRD) and grazing incidence wide-angle X-ray scattering (GIWAXS) (see **Figure 1**a and b, respectively). GIXRD was measured at a Bruker D8 Discover diffractometer, which uses Cu-K_α radiation (λ = 1.54 Å) and a scintillation counter. The angle of incidence was kept constant at approximately $\omega \approx 0.2°$ while the reflection angle 2θ was scanned from 3−90° in angular steps of 0.1°, using a 30 s sampling time. Additionally, the background was measured at a smaller angle of incidence so that X-rays were totally reflected at the interface between air and organic thin film. All measurements shown were background-corrected (cf. Ref. [17] for more details). Due to the small incident angle, the spot size is several mm. With such a large area contributing to the scattering of X-rays, Bragg reflections are broadened compared to the conventional specular geometry. The instrument response is estimated to FWHM ≈ 0.6°, which leads to an uncertainty of ≈ 0.1° on the determined peak position.[18]

2D-GIWAXS measurements were performed at the Stanford Synchrotron Radiation Lightsource (SSRL), beamline 11-3, at an energy of 12.735 keV using a MAR2300 image plate detector for recording. The incident angle was kept constant at ω = 0.12°. 2D-GIWAXS data are isotropically converted to *q*-values and are further analyzed using the software WxDiff.[14]

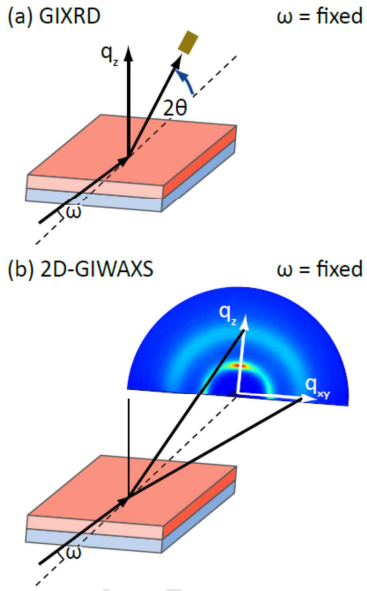

Figure 1. *Experimental setup for measuring (a) GIXRD and (b) GIWAXS. For both measurements, the incident angle ω was kept constant.*

3. Results and Discussion

3.1. Film structure

For our study, $Ir(ppy)_3$ and $Ir(ppy)_2(acac)$ are doped into either a CBP or TCTA matrix. The doping concentration is varied from 0 wt% (i.e. pure matrix) via 20 wt% and 50 wt% to 100 wt% (i.e. pure emitter). Compared to host-guest systems used in OLEDs, we need relatively high

concentrations here since lower concentrations would diminish the relatively weak X-ray signal too much. All thin-film samples are measured without encapsulation under ambient conditions. Previous studies have shown that the molecular arrangement and, hence, X-ray measurements, are not influenced by storage and measurement in air.[18]

In the following, grazing incidence X-ray diffraction (GIXRD) measurements are discussed in the out-of-plane direction, i.e. perpendicular to the substrate. **Figure 2**a and b show the results for $Ir(ppy)_3$ and $Ir(ppy)_2(acac)$ as pure films and when doped into CBP at different concentrations. The pure emitter films show a distinct peak at around 11°, which indicates the presences of crystallites. In addition, the weak shoulder at approximately 22° originating from diffusely scattered radiation suggests the presence of additional amorphous regions in the film. In contrast, the GIXRD spectra of pure CBP and TCTA only show the shoulder at 22°, indicating that both matrix materials have an amorphous morphology. For films containing one of the emitters doped into either of the two matrix materials, the diffraction peak at 11° decreases, but remains visible down to a doping concentration of 20 wt%. This leads us to the conclusion that $Ir(ppy)_3$ and $Ir(ppy)_2(acac)$ form crystalline grains also when embedded into a matrix, at least down to a concentration of 20 wt%. Since the concentrations of $Ir(ppy)_3$ and $Ir(ppy)_2(acac)$ used in OLEDs are typically around 8 wt%, we also tested TCTA films with 8 wt% of $Ir(ppy)_3$ or $Ir(ppy)_2(acac)$. However, we did not observe a diffraction peak for this low concentration. This implies that at 8 wt% molecular aggregation is either reduced or that a lower amount and possibly smaller size of crystallites means that their diffraction peak can no longer be resolved. In reality, a combination of both effects is likely. In the absence of other options to study aggregation with XRD, we therefore resorted to extrapolating results and drawing conclusions from the higher concentration samples.

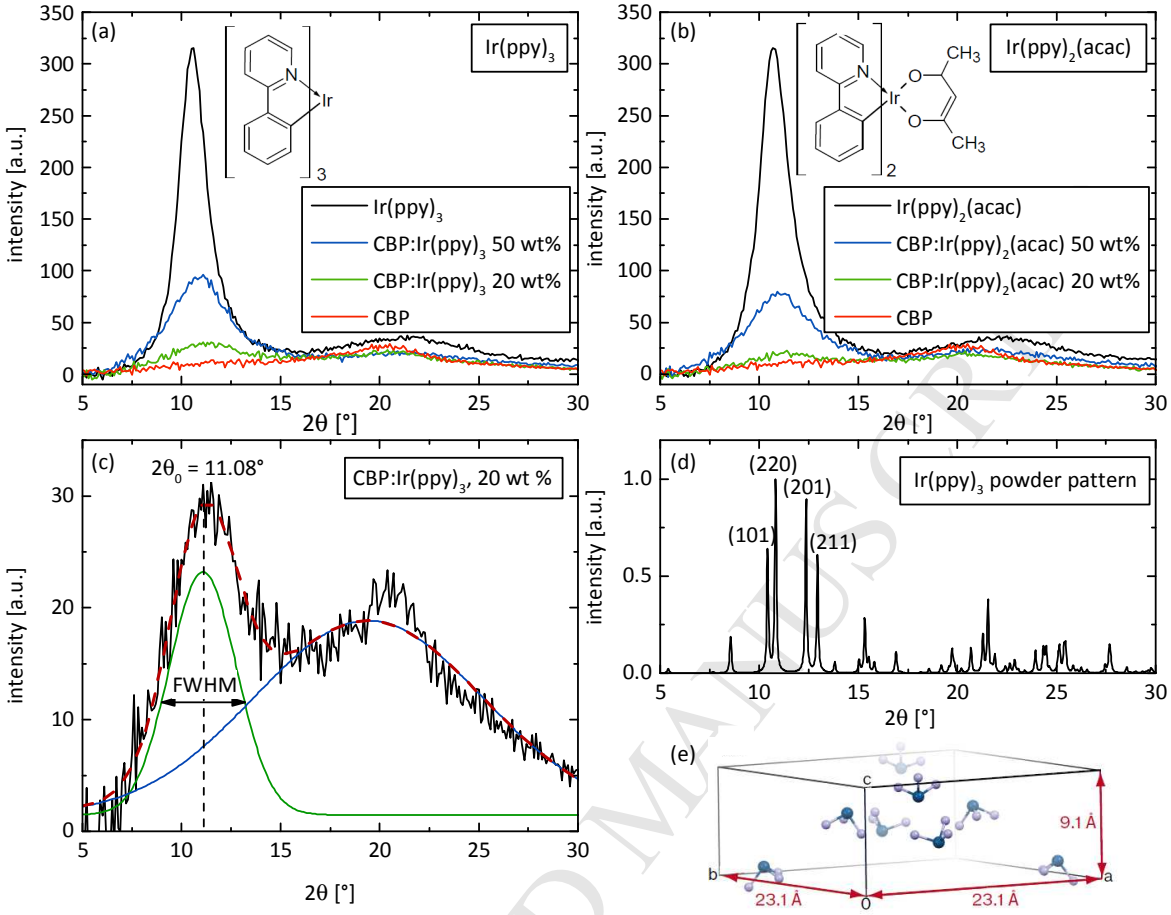

Figure 2. *XRD measurements of thin films containing (a) $Ir(ppy)_3$ and (b) $Ir(ppy)_2(acac)$ as a guest doped into a CBP host matrix at different concentrations. (c) GIXRD spectrum of CBP:$Ir(ppy)_3$ at 20 wt% doping concentration (black line) together with a fit (red dashed line) that is composed of two individual Gauss functions, one for the Bragg reflection (green line) and one to approximate the amorphous halo (blue line). (d) Literature powder diffraction pattern of $Ir(ppy)_3$ with indication of the four main peaks. Figure drawn from data given in Ref.* [19]. *(e) Packing diagram of $Ir(ppy)_3$ showing the unit cell containing eight molecules. Molecules are outlined by their iridium cores and the three nitrogen atoms. The spatial depth of the molecules is indicated by decreasing color intensity.*

According to Bragg's law, the diffraction angle θ is inversely proportional to the distance d of the repeating structures:

$$n\,\lambda = 2d\,sin\,\theta, \quad (1)$$

where λ is the wavelength of the X-rays and n is an integer. To extract the peak position and full width at half maximum (FWHM) from the GIXRD data, all spectra are fitted with two Gauss functions (see Figure 2c). This ensures that the 22° peak caused by diffusely scattered radiation does not interfere with the position of the main peak. The results of all fits and the associated errors are summarized in **Table 1**.

Table 1. *Diffraction angle $2\theta_0$ of the main X-ray reflex and coherence length L_c calculated from the peak width via the Scherrer equation (Eq. (2)). Errors are calculated from the standard deviation of the fits and the instrumental response.*

material	$Ir(ppy)_3$		$Ir(ppy)_2(acac)$	
	$2\theta_0$ [°]	L_c [nm]	$2\theta_0$ [°]	L_c [nm]
guest 100 wt%	10.60±0.10	4.38±0.26	10.82±0.10	3.81±0.21
TCTA:guest 50 wt%	10.75±0.10	2.07±0.07	10.99±0.12	1.43±0.05
TCTA:guest 20 wt%	10.95±0.12	1.49±0.06	12.40±0.14	1.24±0.06
CBP:guest 50 wt%	10.86±0.10	2.46±0.10	10.98±0.10	2.26±0.08
CBP:guest 20 wt%	11.08±0.11	2.22±0.12	11.17±0.12	2.09±0.13

Compared to the $Ir(ppy)_3$ peak, which is located at (10.60 ± 0.10)°, the peak in $Ir(ppy)_2(acac)$ is positioned at (10.82±0.10)°, i.e. there is a small yet significant difference in peak position. We

also observe that the diffraction peak shifts to higher angles as the emitter concentration is reduced, which implies that emitter aggregates become smaller with reducing concentration.

For comparison, Figure 2d shows the powder X-ray diffraction pattern of $Ir(ppy)_3$ as reported in the literature (data provided by Berger *et al.*, Ref. [19], c.f. Cambridge Crystallographic Database entry CCDC-747921). Two peaks are observed in the close vicinity of the thin-film diffraction peak observed in our measurement. The smaller peak at 10.42° originates from diffraction at the (101)-plane and the larger peak at 10.82°, which is also the most intense peak of the powder spectrum, is associated with scattering at the (220)-plane. In an independent set of measurements, Takayasu *et al.*[20] found the (220)-peak to be positioned at 10.72° which leads them to assume a slightly larger crystallite size than Berger *et al*. (Both groups however conclude that the space group of the $Ir(ppy)_3$ crystallites is acentric tetragonal $P\bar{4}2_1c$.) Although neither of the two peaks from the powder spectrum fits exactly to the observed thin-film peak, it is likely that the thin-film peak originates from reflection at the (220)-plane. This is because the (220)-peak is the most intense peak in the powder spectrum, and also because for decreasing $Ir(ppy)_3$ concentrations the position of the peak in the thin-film diffraction data agrees much better with the (220)-peak from the powder data than with the (101)-peak. Figure 2e shows the crystal packing of the $Ir(ppy)_3$ unit cell, which contains eight molecules. The C_3 symmetry axis of the $Ir(ppy)_3$ molecules and their large permanent dipole moment (magnitude, 6.4 D) lie approximately parallel to the *c* axis of the unit cell, pointing in the direction of the nitrogen atoms.[7] Within the crystal, groups of four molecules always form a tetramer. Every second molecule has different chirality meaning that their permanent dipole moments oppose in direction and will compensate in far-field.[19] It should be noted that $Ir(ppy)_3$ is polymorphic, i.e. the crystallographic data of vacuum sublimed $Ir(ppy)_3$-films that we showed above is

different from the crystal structure found for single crystals grown by slow evaporation from solution.[21] The crystal structure for $Ir(ppy)_2(acac)$ has so far only been measured for crystals grown from solution.[22,23] Given that our $Ir(ppy)_2(acac)$ films are vacuum sublimed and considering the polymorphism observed for $Ir(ppy)_3$ it therefore remains unclear where the $Ir(ppy)_2(acac)$ thin-film diffraction peak, which occurs at a similar position as the $Ir(ppy)_3$ peak, originates from.

3.2. Molecular aggregation

Studies of the film morphology not only give valuable insight into molecular orientation but may also provide insight into aggregation, which can enhance the rate of exciton annihilation and thus typically increases the efficiency roll-off of OLEDs at high current densities.[24,25] In order to compare the amount of molecular aggregation between the two emitters, the size of the crystallite grains is approximated with the Scherrer equation, which correlates the FWHM $\Delta(2\theta_0)$ of the diffraction peak (located at $2\theta_0$) with the coherence length L_c:[15]

$$L_c = \frac{K\lambda}{\cos((2\theta_0)/2)\Delta(2\theta_0)}. \quad (2)$$

Here, K denotes a shape factor that can be approximated as 1. The resulting coherence length is 4.4 nm and 3.8 nm for the 100 wt% samples of $Ir(ppy)_3$ and $Ir(ppy)_2(acac)$, respectively (Table 1). The L_c value predicted by Eq. (2) decreases for films in which the emitter molecules are embedded into a host. We note that our calculation yields the coherence length in the out-of-plane direction and thus approximates the size of aggregates perpendicular to the substrate. The dimensions in the in-plane extension (parallel to the substrate) may therefore well be different.

For all host-guest combinations studied here, L_c is higher for $Ir(ppy)_3$ than for $Ir(ppy)_2(acac)$ and higher for CBP than for TCTA as host. A longer coherence length correlates with larger crystallite grains and therefore indicates that $Ir(ppy)_3$ forms larger aggregates than $Ir(ppy)_2(acac)$, as has been previously suggested by Reineke *et al.*[16]. However, the calculated coherence length only gives a lower limit for the size of aggregates. For instance, a distortion of the molecular arrangement due to cumulative disorder leads to small estimates of grain size although a larger molecular arrangement is present.[15] In addition, only the crystallite components of the materials can be considered while amorphous parts with possibly different structure and size are neglected. Although doping concentrations were only investigated down to 20 wt%, aggregation is likely to also be present for lower concentrations even though a (220)-Bragg reflection was not observed for these.[26] Note that a diffraction peak can only be observed if the crystal structure is preserved within aggregates, which requires at least one complete unit cell.

3.3. Molecular orientation

Up to now, we have only discussed scattering in out-of-plane direction as observed by GIXRD. In order to learn more about the orientation of molecules on the substrate, we performed 2D grazing incidence wide-angle X-ray scattering (2D-GIWAXS) measurements. Data for $Ir(ppy)_3$- and $Ir(ppy)_2(acac)$-doped CBP films are shown in **Figure 3** (again at doping concentrations of 0, 20, 50 and 100 wt%). Here, q_z denotes the out-of-plane direction and q_{xy} the in-plane direction. The scattering vector q_z relates to the diffraction angle 2θ via[27]

$$q_z = \frac{2\pi}{\lambda}(\sin\omega + \sin(2\theta - \omega)). \quad (3)$$

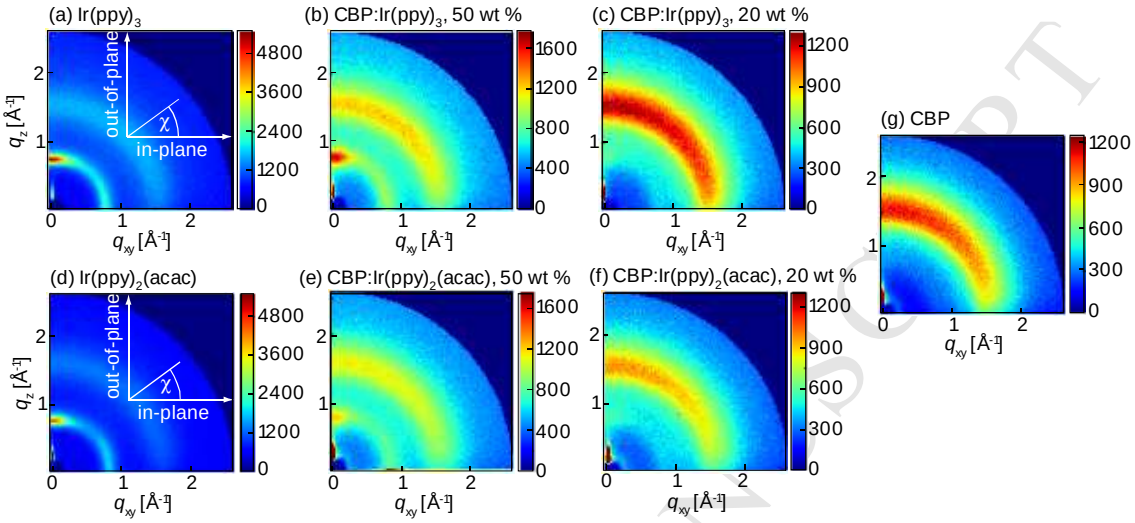

Figure 3. *2D-GIWAXS measurements on thin films of $Ir(ppy)_3$ and $Ir(ppy)_2(acac)$ doped into CBP at different concentrations. (a) plain $Ir(ppy)_3$ film; (b) 50 wt% $Ir(ppy)_3$ in CBP; (c) 20 wt% $Ir(ppy)_3$ in CBP; (d) plain $Ir(ppy)_2(acac)$ film; (e) 50 wt% $Ir(ppy)_2(acac)$ in CBP; (e) 20 wt% $Ir(ppy)_2(acac)$ in CBP; (g) plain CBP film. Shown is a false color plot of the scattering intensity as a function of the in-plane and out-of-plane scattering vectors q_{xy} and q_z.*

An isotropic orientation of the crystallites would appear as a ring in the 2D-measurements, whereas spots indicate strong orientation.[15] For the pure $Ir(ppy)_3$ and $Ir(ppy)_2(acac)$ films, an intense spot-shaped peak is observed in out-of-plane direction at q = 0.75 $Å^{-1}$ with further intensity along a ring. The intensity of the peak decreases when $Ir(ppy)_3$ and $Ir(ppy)_2(acac)$ are doped into CBP. There is also a second broad halo ring at q = 1.5 $Å^{-1}$. The diffraction patterns are similar for $Ir(ppy)_3$ and $Ir(ppy)_2(acac)$.

Before analyzing the 2D-GIWAXS data further, we compared the scatting in out-of-plane direction against the results from the earlier GIXRD measurement. **Figure 4**a shows the out-of-plane component of the 2D-GIWAXS signal for the pure $Ir(ppy)_3$ and $Ir(ppy)_2(acac)$ films, summed over the polar angle χ from $80° < \chi < 100°$ and compares this data to the GIXRD measurements. The 11° diffraction peak from the GIXRD measurement is clearly reproduced by the peak and ring at $q = 0.75$ Å^{-1}, showing that the main 2D-GIWAXS peak is associated with (220)-scattering. The broad halo ring at $q = 1.5$ Å^{-1} is related to the second peak in GIXRD measurements at around 22° confirming the presence of diffusely scattered radiation due to amorphous regions in the film.[17] There are slight deviations in the width of the first peak between the GIXRD and 2D-GIWAXS measurement and a more pronounced difference in the intensity of the second peak. These deviations are mainly due to missing background information for the 2D-GIWAXS data. Furthermore, the summation over a range of polar angles ($80° < \chi < 100°$) leads to a change in the intensity ratio between the first and the second peak and potentially a small amount of background may have been collected from the underlying glass substrate as well. Nevertheless, the measurements still allow a qualitative comparison.

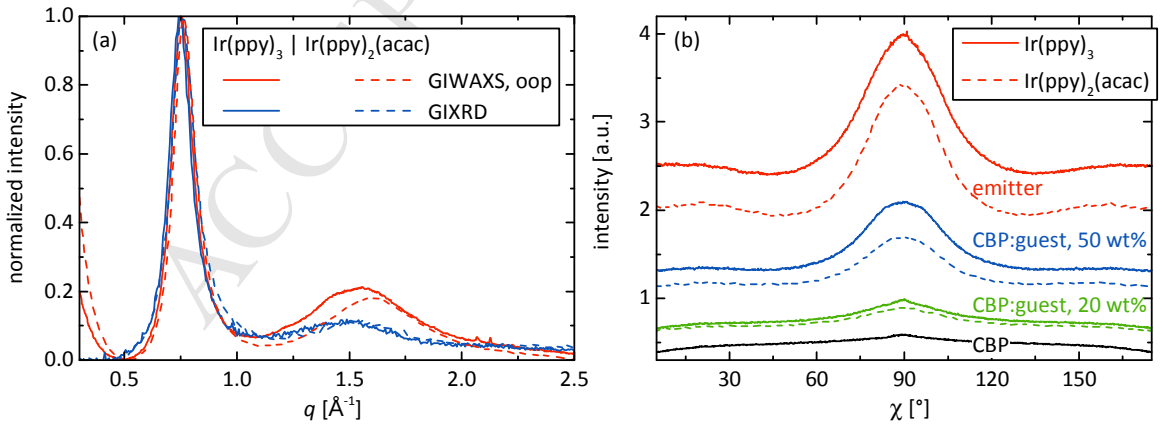

Figure 4. *(a) Comparison of the out-of-plane (oop)-component of the 2D-GIWAXS data, calculated by summation over all χ between 80° and 100°, to the GIXRD-measurements. (b)*

Intensity of the 'inner ring' of 2D-GIWAXS data for the films shown in Fig. 2 as a function of the angle χ, intensity summed over 0.6 $Å^{-1} \leq q \leq 1.0$ $Å^{-1}$.

Next, we investigated the change in the scattering intensity at q = 0.75 $Å^{-1}$ with polar angle. Figure 4b shows the scattering signal for all films as a function of the polar angle χ, summed over all q from 0.6 $Å^{-1}$ to 1.0 $Å^{-1}$. For the pure $Ir(ppy)_3$ film there is a pronounced peak in out-of-plane direction (χ = 90°, FWHM ≈ 30°), which indicates that the $Ir(ppy)_3$ crystallites are preferentially oriented with their (220)-plane in out-of-plane direction. A similar behavior is found for the $Ir(ppy)_2(acac)$ film. For films of $Ir(ppy)_3$ and $Ir(ppy)_2(acac)$ doped into CBP the overall intensity is significantly reduced, but the FWHM of roughly 30° is preserved suggesting that the preferential orientation is retained. For the pure $Ir(ppy)_3$ and $Ir(ppy)_2(acac)$ films, there is also a slight increase in intensity in in-plane direction (χ = 90°), which may indicate that a fraction of the crystallites is rotated by approximately 90°. The trend vanishes for lower emitter concentrations and is not present in the pure CBP film.

4. Conclusions

The 2D-GIWAXS measurements show that, although the degree of order is relatively low and the crystallite size is small, there is a preferential orientation of both $Ir(ppy)_3$ and $Ir(ppy)_2(acac)$ in thin vacuum sublimed films. For $Ir(ppy)_3$, we found that crystallites are predominantly oriented with the (220)-plane parallel to the substrate. Hence, one can conclude that the symmetry axis of the $Ir(ppy)_3$ molecules is roughly parallel to the substrate as illustrated in **Figure 5**. This orientation is preserved when doping $Ir(ppy)_3$ into a matrix, at least for the concentrations investigated here. For $Ir(ppy)_2(acac)$ the experimental observations are similar but

due to its unknown crystal structure the exact molecular orientation with respect to the substrate cannot be determined at this stage.

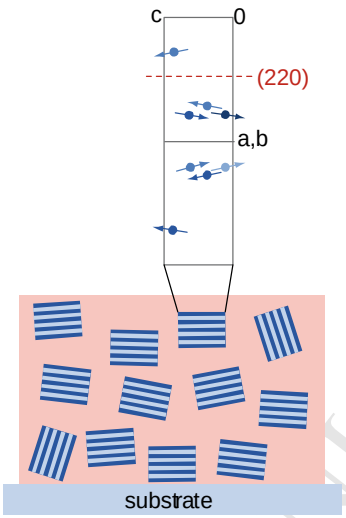

Figure 5. *Schematic illustration of the orientation of Ir(ppy)$_3$ crystallites embedded in a matrix. The top part of the sketch shows the crystal structure of the Ir(ppy)$_3$ unit cell with the (220)-plane parallel to the substrate. The symmetry axis of the Ir(ppy)$_3$ molecule and its permanent dipole moment, which both point along the direction of the blue arrows, are oriented roughly in-plane. The spatial depth of the molecules is indicated by decreasing color intensity. A small fraction of the crystallites sketched in the lower part of the illustration is turned by approximately 90° with respect to the majority of the crystallites.*

Very recently, Lee *et al.* performed molecular density (MD) simulations of CBP films comprising Ir(ppy)$_3$ and Ir(ppy)$_2$(acac) as emitters, respectively.[28] For both emitters they found a preferential orientation of the emitter symmetry axis with respect to the substrate. In contrast to our experimental findings, however, the symmetry axes of Ir(ppy)$_3$ molecules were aligned preferentially perpendicular to the substrate. A similar set of MD simulations on the same host-guest system that was very recently performed by Moon *et al.* revealed no preferential

orientation.[29] Both sets of MD simulations do not take aggregation of emitter molecules into account but this is likely to be a relevant factor for the orientation observed in experiments.

Our measurements reveal that molecular orientation is particularly pronounced for pure films of the emitter molecules and it seems to be an intrinsic property of the material growth during thermal evaporation. The observation that the crystallites and permanent dipoles of both iridium complexes investigated here are oriented in thin evaporated films is particularly significant given that transition dipole moments only show a preferential orientation for $Ir(ppy)_2(acac)$ but were found to be isotropic for $Ir(ppy)_3$.[3] Quantum chemical calculations can give an indication as to how the transition dipoles are oriented with respect to the symmetry axis of the molecule, even though it is not yet clear if this yields reliable results and to which extend the environment influences the orientation of the transition dipole vector.[28] Using this approach, Moon *et al*. recently found that the transition dipole moments of the three triplet sublevels of $Ir(ppy)_3$ point from the iridium core to the three ligands and are mutually orthogonal.[30] Hence, the three transition dipoles cancel each other, which leads to the isotropic dipole orientation that was previously observed in OLEDs.

For $Ir(ppy)_2(acac)$, instead, the two transition dipole vectors point towards the phenylpyridine ligands and, thus, lie roughly in the same plane, perpendicular to the symmetry axis.[23,28] Together with the orientation of $Ir(ppy)_2(acac)$ molecules on the substrate that we found in our 2D-GIWAXS study, this would explain the observed preferential horizontal orientation of the transition dipole moment in OLEDs.

In conclusion, we found that both $Ir(ppy)_3$ and $Ir(ppy)_2(acac)$ form crystalline grains which exhibit a preferential orientation on the substrate. When embedding the molecules into a matrix,

aggregates of emitter molecules are formed, which retain the molecular orientation. Hence, the emitter orientation seems to be an intrinsic property of the film formation process.

ACKNOWLEDGMENT

We thank Dr. Lutz Wilde at Fraunhofer IPMS, Center Nanoelectronic Technologies, Dresden, for carrying out the GIXRD measurements and Dr. Philipp Liehm and Prof. Stefan C. B. Mannsfeld for fruitful discussions. This work received funding from the European Community Seventh Framework Programme under Grant Agreement No. FP7 267995 (NUDEV) and from the European Social Fund and the Free State of Saxony through the OrganoMechanics project. CM acknowledges funding from the Graduate Academy of the TU Dresden and by the European Commission through a Marie Skłodowska-Curie Individual Fellowship (703387).

DATA AVAILABILITY

The research data supporting this publication can be accessed at http://dx.doi.org/10.17630/2dc12142-818e-4c40-8ae8-6ef03a75e49f.

REFERENCES

[1] T.D. Schmidt, D.S. Setz, M. Flämmich, J. Frischeisen, D. Michaelis, B.C. Krummacher, N. Danz, W. Brütting, Evidence for non-isotropic emitter orientation in a red phosphorescent organic light-emitting diode and its implications for determining the emitter's radiative quantum efficiency, Appl. Phys. Lett. 99 (2011) 163302. doi:10.1063/1.3653475.

[2] M. Flämmich, J. Frischeisen, D.S. Setz, D. Michaelis, B.C. Krummacher, T.D. Schmidt, W. Brütting, N. Danz, Oriented phosphorescent emitters boost OLED efficiency, Org.

Electron. 12 (2011) 1663–1668. doi:10.1016/j.orgel.2011.06.011.

[3] P. Liehm, C. Murawski, M. Furno, B. Lüssem, K. Leo, M.C. Gather, Comparing the emissive dipole orientation of two similar phosphorescent green emitter molecules in highly efficient organic light-emitting diodes, Appl. Phys. Lett. 101 (2012) 253304. doi:10.1063/1.4773188.

[4] D. Yokoyama, Molecular orientation in small-molecule organic light-emitting diodes, J. Mater. Chem. 21 (2011) 19187. doi:10.1039/c1jm13417e.

[5] M.C. Gather, S. Reineke, Recent advances in light outcoupling from white organic light-emitting diodes, J. Photonics Energy. 5 (2015) 57607. doi:10.1117/1.JPE.5.057607.

[6] K.-H. Kim, S. Lee, C.-K. Moon, S.-Y. Kim, Y.-S. Park, J.-H. Lee, J.W. Lee, J. Huh, Y. You, J.-J. Kim, Phosphorescent dye-based supramolecules for high-efficiency organic light-emitting diodes, Nat. Commun. 5 (2014) 4769. doi:10.1038/ncomms5769.

[7] A. Graf, P. Liehm, C. Murawski, S. Hofmann, K. Leo, M.C. Gather, Correlating the transition dipole moment orientation of phosphorescent emitter molecules in OLEDs with basic material properties, J. Mater. Chem. C. 2 (2014) 10298. doi:10.1039/C4TC00997E.

[8] M.J. Jurow, C. Mayr, T.D. Schmidt, T. Lampe, P.I. Djurovich, W. Brütting, M.E. Thompson, Understanding and predicting the orientation of heteroleptic phosphors in organic light-emitting materials, Nat. Mater. 15 (2015) 85–91. doi:10.1038/nmat4428.

[9] M. Flämmich, M.C. Gather, N. Danz, D. Michaelis, A.H. Bräuer, K. Meerholz, A. Tünnermann, Orientation of emissive dipoles in OLEDs: Quantitative in situ analysis, Org. Electron. 11 (2010) 1039–1046. doi:10.1016/j.orgel.2010.03.002.

[10] J. Frischeisen, D. Yokoyama, C. Adachi, W. Brütting, Determination of molecular dipole orientation in doped fluorescent organic thin films by photoluminescence measurements,

Appl. Phys. Lett. 96 (2010) 73302. doi:10.1063/1.3309705.

[11] R. Mac Ciarnain, D. Michaelis, T. Wehlus, A.F. Rausch, S. Wehrmeister, T.D. Schmidt, W. Brütting, N. Danz, A. Bräuer, A. Tünnermann, Plasmonic Purcell effect reveals obliquely ordered phosphorescent emitters in Organic LEDs, Sci. Rep. 7 (2017) 1826. doi:10.1038/s41598-017-01701-8.

[12] K.-H. Kim, J.-L. Liao, S.W. Lee, B. Sim, C.-K. Moon, G.-H. Lee, H.J. Kim, Y. Chi, J.-J. Kim, Crystal Organic Light-Emitting Diodes with Perfectly Oriented Non-Doped Pt-Based Emitting Layer, Adv. Mater. 28 (2016) 2526–2532. doi:10.1002/adma.201504451.

[13] L. Li, Q. Tang, H. Li, X. Yang, W. Hu, Y. Song, Z. Shuai, W. Xu, Y. Liu, D. Zhu, An ultra closely pi-stacked organic semiconductor for high performance field-effect transistors, Adv. Mater. 19 (2007) 2613. doi:10.1002/adma.200700682.

[14] S.C.B. Mannsfeld, M.L. Tang, Z. Bao, Thin film structure of triisopropylsilylethynyl-functionalized pentacene and tetraceno[2,3-b]thiophene from grazing incidence x-ray diffraction, Adv. Mater. 23 (2011) 127. doi:10.1002/adma.201003135.

[15] J. Rivnay, S.C.B. Mannsfeld, C.E. Miller, A. Salleo, M.F. Toney, Quantitative Determination of Organic Semiconductor Microstructure from the Molecular to Device Scale, Chem. Rev. 112 (2012) 5488–5519. doi:10.1021/cr3001109.

[16] S. Reineke, T.C. Rosenow, B. Lüssem, K. Leo, Improved High-Brightness Efficiency of Phosphorescent Organic LEDs Comprising Emitter Molecules with Small Permanent Dipole Moments., Adv. Mater. 22 (2010) 3189. doi:10.1002/adma.201000529.

[17] C. Elschner, A.A. Levin, L. Wilde, J. Grenzer, C. Schroer, K. Leo, M. Riede, Determining the C60 molecular arrangement in thin films by means of X-ray diffraction, J. Appl. Crystallogr. 44 (2011) 983–990. doi:10.1107/S002188981103531X.

[18] C. Elschner, Structural Investigations of Disordered Organic Thin Films, Technische Universität Dresden, 2013. http://d-nb.info/1037923774.

[19] R.J.F. Berger, H.G. Stammler, B. Neumann, N.W. Mitzel, Fac-Ir(ppy)3: Structures in the gas-phase and of a new solid modification, Eur. J. Inorg. Chem. 2010 (2010) 1613–1617. doi:10.1002/ejic.201000125.

[20] S. Takayasu, T. Suzuki, K. Shinozaki, Intermolecular interactions and aggregation of fac-tris(2-phenylpyridinato-C2,N)iridium(III) in nonpolar solvents., J. Phys. Chem. B. 117 (2013) 9449–56. doi:10.1021/jp403974h.

[21] J. Breu, P. Stössel, S. Schrader, A. Starukhin, W.J. Finkenzeller, H. Yersin, Crystal Structure of fac − Ir(ppy)3 and Emission Properties under Ambient Conditions and at High Pressure, Chem. Mater. 17 (2005) 1745–1752. doi:10.1021/cm0486767.

[22] S. Lamansky, P. Djurovich, D. Murphy, F. Abdel-Razzaq, R. Kwong, I. Tsyba, M. Bortz, B. Mui, R. Bau, M.E. Thompson, Synthesis and Characterization of Phosphorescent Cyclometalated Iridium Complexes, Inorg. Chem. 40 (2001) 1704–1711. doi:10.1021/ic0008969.

[23] J. Frey, B.F.E. Curchod, R. Scopelliti, I. Tavernelli, U. Rothlisberger, M.K. Nazeeruddin, E. Baranoff, Structure-property relationships based on Hammett constants in cyclometalated iridium(iii) complexes: their application to the design of a fluorine-free FIrPic-like emitter., Dalt. Trans. 43 (2014) 5667–79. doi:10.1039/c3dt52739e.

[24] S. Reineke, G. Schwartz, K. Walzer, M. Falke, K. Leo, Highly phosphorescent organic mixed films: The effect of aggregation on triplet-triplet annihilation, Appl. Phys. Lett. 94 (2009) 163305. doi:10.1063/1.3123815.

[25] C. Murawski, K. Leo, M.C. Gather, Efficiency Roll-Off in Organic Light-Emitting

Diodes, Adv. Mater. 25 (2013) 6801. doi:10.1002/adma.201301603.

[26] C. Murawski, C. Elschner, S. Lenk, S. Reineke, M.C. Gather, Orientation of OLED Emitter Molecules Revealed by XRD, in: Light. Energy Environ., OSA, Washington, D.C., 2016: p. SSW2D.7. doi:10.1364/SSL.2016.SSW2D.7.

[27] U. Pietsch, V. Holý, T. Baumbach, High-Resolution X-Ray Scattering, Springer-Verlag New York, 2004.

[28] T. Lee, B. Caron, M. Stroet, D.M. Huang, P.L. Burn, A.E. Mark, The molecular origin of anisotropic emission in an organic light-emitting diode, Nano Lett. (2017). doi:10.1021/acs.nanolett.7b03528.

[29] C. Moon, J. Kim, K.-H. Kim, Unraveling the origin of the orientation of Ir complexes doped in organic semiconducting layers, in: F. So, C. Adachi, J.-J. Kim (Eds.), Proc. SPIE, SPIE, 2017: p. 1036213. doi:10.1117/12.2273505.

[30] C.-K. Moon, K.-H. Kim, J.W. Lee, J.-J. Kim, Influence of Host Molecules on Emitting Dipole Orientation of Phosphorescent Iridium Complexes, Chem. Mater. 27 (2015) 2767–2769. doi:10.1021/acs.chemmater.5b00469.

TABLE OF CONTENTS GRAPHIC

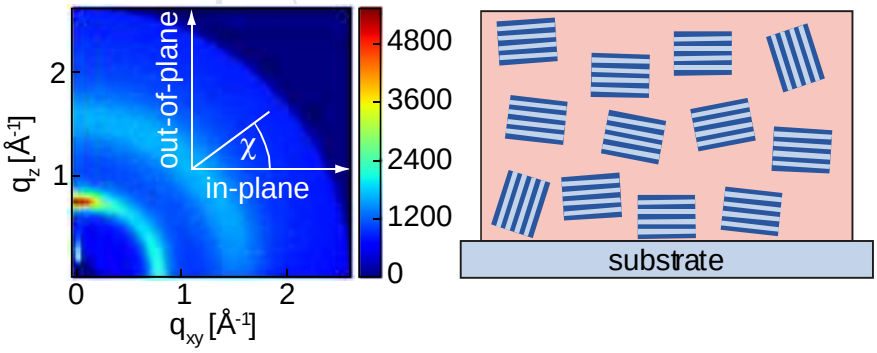

- $Ir(ppy)_3$ and $Ir(ppy)_2(acac)$ form small crystallite grains.
- Grains show a preferred orientation on the substrate.
- $Ir(ppy)_3$ molecules orient roughly parallel to the substrate.
- Crystallite formation and orientation preserve when emitters are doped into host.